

RESEARCH ARTICLE | FEBRUARY 12 2024

Dissimilar thermal transport properties in κ -Ga₂O₃ and β -Ga₂O₃ revealed by homogeneous nonequilibrium molecular dynamics simulations using machine-learned potentials **FREE**

Special Collection: [Machine Learning for Thermal Transport](#)

Xiaonan Wang ; Jinfeng Yang ; Penghua Ying ; Zheyong Fan ; Jin Zhang ; Huarui Sun 

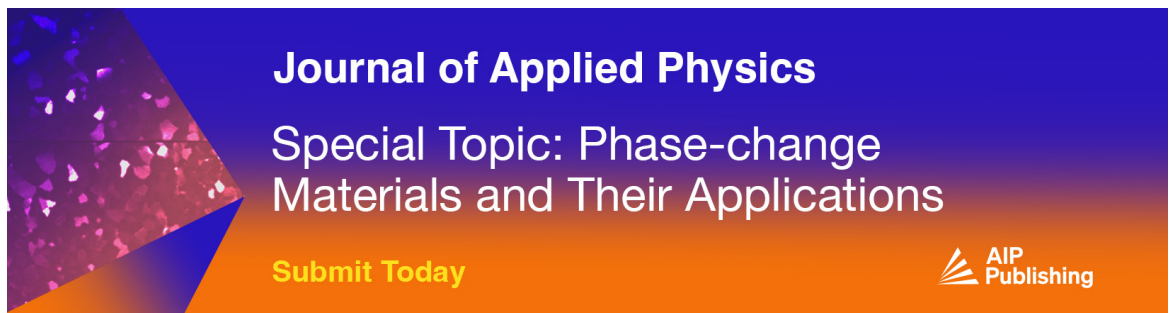


J. Appl. Phys. 135, 065104 (2024)


<https://doi.org/10.1063/5.0185854>



CrossMark



Journal of Applied Physics
Special Topic: Phase-change Materials and Their Applications
Submit Today



Dissimilar thermal transport properties in κ -Ga₂O₃ and β -Ga₂O₃ revealed by homogeneous nonequilibrium molecular dynamics simulations using machine-learned potentials

Cite as: J. Appl. Phys. 135, 065104 (2024); doi: 10.1063/5.0185854

Submitted: 2 November 2023 · Accepted: 18 January 2024 ·

Published Online: 12 February 2024



Xiaonan Wang,¹ Jinfeng Yang,¹ Penghua Ying,^{1,a)} Zheyong Fan,² Jin Zhang,¹ and Huarui Sun^{1,3,a)}

AFFILIATIONS

¹School of Science, Harbin Institute of Technology, Shenzhen 518055, People's Republic of China

²College of Physical Science and Technology, Bohai University, Jinzhou 121013, People's Republic of China

³Ministry of Industry and Information Technology Key Laboratory of Micro-Nano Optoelectronic Information System, Harbin Institute of Technology, Shenzhen 518055, People's Republic of China and Collaborative Innovation Center of Extreme Optics, Shanxi University, Taiyuan 030006, People's Republic of China

Note: This paper is part of the special topic, Machine Learning for Thermal Transport.

a) Authors to whom correspondence should be addressed: hityingph@163.com and huarui.sun@hit.edu.cn

ABSTRACT

The lattice thermal conductivity (LTC) of Ga₂O₃ is an important property due to the challenge in the thermal management of high-power devices. In this work, we develop machine-learned neuroevolution potentials (NEPs) for single-crystalline β -Ga₂O₃ and κ -Ga₂O₃ and demonstrate their accuracy in modeling thermal transport properties. Combining NEP-driven homogeneous non-equilibrium molecular dynamics simulations with tensor analysis, we determine the spatial distributions of LTCs for two Ga₂O₃ crystals, showing dissimilar thermal behaviors. Specifically, β -Ga₂O₃ shows isotropic thermal transport properties, with the LTCs along [100], [010], and [001] directions being predicted to be 10.3 ± 0.2 , 19.9 ± 0.2 , and 12.6 ± 0.2 W/(m K), respectively, consistent with previous experimental measurements. For κ -Ga₂O₃, our predictions suggest nearly isotropic thermal transport properties, with the LTCs along [100], [010], and [001] being estimated to be 4.5 ± 0.1 , 3.9 ± 0.1 , and 4.0 ± 0.1 W/(m K). The reduced LTC of κ -Ga₂O₃ vs β -Ga₂O₃ stems from its restricted low-frequency phonons up to 5 THz. Furthermore, we find that the β phase exhibits a typical temperature dependence slightly stronger than $\sim T^{-1}$, whereas the κ phase shows a weaker temperature dependence, ranging from $\sim T^{-0.5}$ to $\sim T^{-0.7}$.

Published under an exclusive license by AIP Publishing. <https://doi.org/10.1063/5.0185854>

I. INTRODUCTION

Ultra-wide bandgap semiconductors, such as Ga₂O₃, diamond, and AlN, have also become the focus of attention materials for next-generation electronics and optoelectronics. Owing to a bandgap of about 5 eV, exceptional breakdown electrical field, and cost-effective production, Ga₂O₃ offers considerable promise for ultrahigh power device applications.^{1–3} However, the lattice thermal conductivity (LTC) of Ga₂O₃ is subpar, leading to pronounced

heat dissipation issues in certain semiconductor devices.¹ Understanding the phonon thermal transport in Ga₂O₃ is crucial for its practical applications.

The Ga₂O₃ crystal actually exists in five distinct phases: α , β , γ , σ , and ε (sometimes referred to as κ). Of these, the β phase (space group C2/m) is the most stable one, which has been extensively explored for applications in deep-ultraviolet transparent conductive electrodes,⁴ solar blind detectors,^{5,6} high-performance field effect transistors,⁷ Schottky rectifiers,⁸ and high temperature gas

sensors.¹ In recent years, further efforts have been made to overcome the poor thermal stability and immature synthesis methods of other phases. Hexagonal crystal ϵ -Ga₂O₃ (space group P63mc) was reported to be the second most stable phase obtained at low temperatures,^{9,10} whereas subsequent studies claimed that the crystal structure of the polycrystalline form at low temperatures has an orthorhombic structure at the nanoscale (5–10 nm), named κ -Ga₂O₃ (space group Pna21).^{11,12} The strong polarization in κ -Ga₂O₃ is a prominent feature that β -Ga₂O₃ does not possess, which may benefit potential device applications. For example, κ -Ga₂O₃ can form heterojunctions with other semiconductors such as GaN or AlN, and its polarization was utilized to regulate interface transport while effectively alleviating thermal problems.^{13,14} Considering the distinct crystal structures of β and κ -Ga₂O₃, a comparative understanding of the LTC for both phases is essential for their device thermal design, particularly as the κ phase remains unexplored.

Currently, growing large-scale single-crystalline κ -Ga₂O₃ is a challenging endeavor experimentally, and assessing its LTC is anticipated to be even more demanding. From a computational perspective, its LTC can be predicted using atomistic simulation techniques, such as molecular dynamics (MD) simulations^{15–17} and the combination of Boltzmann transport equation (BTE) with the anharmonic lattice dynamics (ALD) method.^{18–20} While atomic interactions can be derived from either empirical potentials or quantum mechanical density functional theory (DFT) calculations, intricate crystals like κ -Ga₂O₃, which possess 40 atoms in their primitive cell, introduce substantial hurdles—accuracy concerns for empirical potentials and computational overhead for DFT. Recently, the prediction of thermal transport properties in materials has been significantly accelerated through the combined use of machine learning approaches and atomistic simulation methods.²¹ Specifically, machine-learned potential (MLP)-based large-scale MD simulations have been demonstrated to be a reliable approach to calculate the LTC of complex crystals including amorphous silicon,²² amorphous HfO₂,²³ amorphous silica,²⁴ metal-organic frameworks,²⁵ and violet phosphorene,²⁶ which can account for phonon anharmonicity to arbitrary order. Several MLPs for Ga₂O₃ have been developed, addressing both the perfect bulk system^{15,19,27} and more intricate, disordered structures.^{28,29}

In this work, we apply the neuroevolution potential (NEP) framework^{30–32} to develop two MLPs on demand for Ga₂O₃ against quantum-mechanical DFT calculations, one for β phase and one for κ phase. We choose the NEP approach here, because this method has been demonstrated to be highly efficient.³² We apply the developed NEPs to perform extensive homogeneous non-equilibrium molecular dynamics (HNEMD) simulations to investigate the LTC of the two phases of Ga₂O₃. Our results show that the LTC of the κ phase is much lower than that of the β phase and exhibits low anisotropy and weak temperature dependence.

II. METHODS

A. Structural model and DFT calculations

All DFT calculations were performed using projected augmented wave method³³ with Perdew–Burke–Ernzerhof functional of generalized gradient approximation³⁴ implemented in the VASP package.^{35,36} The kinetic energy cutoff was set to 520 eV, and the

convergence value for the total energy was 1×10^{-6} eV. The stopping criteria for structural optimizations were that the maximum residual Hellmann–Feynman force on atoms was less than 1×10^{-3} eV/Å. A $10 \times 10 \times 6$ and $10 \times 6 \times 6$ Γ -centered k-point grid was employed for the primitive cell of β -Ga₂O₃ and κ -Ga₂O₃, respectively. Additionally, to validate the accuracy of the MLP, the phonon dispersions of β -Ga₂O₃ and κ -Ga₂O₃ were further calculated on $2 \times 2 \times 2$ and $3 \times 1 \times 1$ supercells, respectively, using the density functional perturbation theory together with the PHONOPY package.³⁷

Meanwhile, according to widely used conventions, we have optimized the corresponding conventional unit cell as the initial cell for the MD simulation. The κ -Ga₂O₃ lattice structure remains unchanged, but the number of atoms in the conventional unit cell of β -Ga₂O₃ is higher than that in the primitive cell. The calculated lattice constants of β -Ga₂O₃ are $a = 12.468$, $b = 3.087$, and $c = 5.716$ Å, while these values for κ -Ga₂O₃ are $a = 5.074$, $b = 8.703$, and $c = 9.309$ Å, which are close to the reported values.^{12,38} As shown in Fig. 1, the conventional unit cell of β -Ga₂O₃ has 20 atoms, while κ -Ga₂O₃ has a relatively large number of 40 atoms. In the calculations of the reference datasets for NEP training, the $2 \times 2 \times 2$ and $2 \times 1 \times 1$ supercells were used for β -Ga₂O₃ and κ -Ga₂O₃, respectively, with $1 \times 4 \times 2$ and $3 \times 3 \times 3$ k-point grids.

B. The NEP model training

We used the identical method to construct the reference datasets for the β and κ phases of Ga₂O₃. The reference structures were obtained by *ab initio* molecular dynamics (AIMD) simulations and random perturbations. For each phase, the AIMD simulations were run under an isothermal ensemble with temperature increasing linearly from 10 to 1000 K for 10 000 steps and a time step of 1 fs. We uniformly extracted 1000 structures from AIMD simulations for each case. For random perturbations, 200 structures were generated with random cell deformations ranging from –4% to 4% and atomic displacements less than 0.1 Å, all based on optimized structures. For both phases, our total dataset has 1200 structures including energy, atomic forces, and virials obtained from DFT calculations as outlined in Sec. II A. We randomly divided the total dataset into a training set of 1000 structures and a test set of 200 structures.

After obtaining the training set and test set, we applied the third generation of the NEP framework³² implemented in GPUMD (version 3.5) to train the MLP for β and κ phases of Ga₂O₃, which were denoted as NEP- β and NEP- κ , respectively. NEP used a feed-forward neural network to represent the site energy with atomic cluster expansion (ACE)³⁹-like descriptor components including radial and angular terms. The parameters of NEP models were optimized using the separable natural evolution strategy (SNES),⁴⁰ with the loss function defined as a weighted sum over the root mean square error (RMSE) values of energy, atomic force, and virial. As shown in Fig. S1 (see the [supplementary material](#)), the RMSEs of energy, force, and virial converge well with increasing training step.

We used the same hyperparameters for these two NEP models. After extensive testing, the selected hyperparameters were

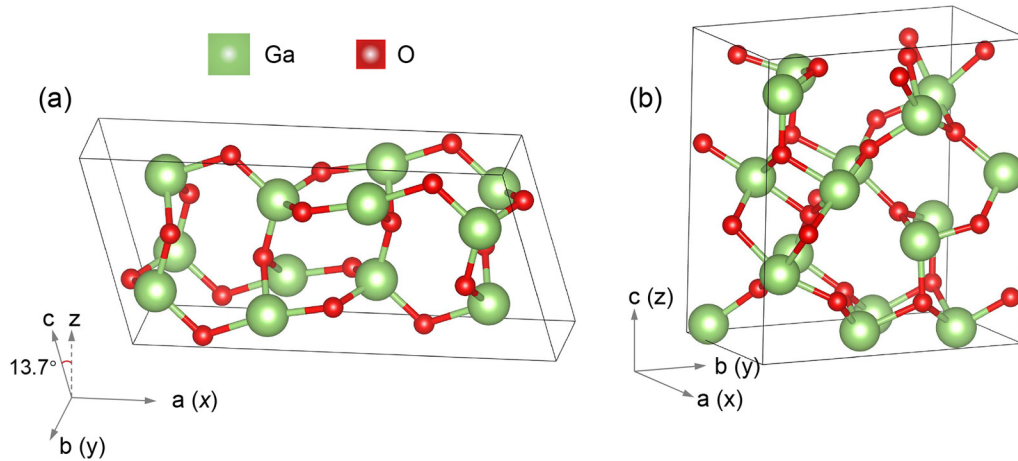


FIG. 1. Crystal structure of the conventional unit cell of (a) β -Ga₂O₃ and (b) κ -Ga₂O₃.

determined as follows: the radial and angular cutoffs are $r_c^R = 8 \text{ \AA}$ and $r_c^A = 4 \text{ \AA}$, respectively. The number of radial and angular descriptor components is $n_{\max}^R + 1 = 9$ and $n_{\max}^A + 1 = 9$, respectively. For angular parameters, we have $l_{\max}^b = 4$ for three-body and $l_{\max}^{4b} = 2$ for four-body terms, respectively. The number of neurons in the hidden layer of the neural network is 50. The size of the population is $N_{\text{pop}} = 50$, and the number of generations is $N_{\text{gen}} = 5 \times 10^5$. The weights of energy, force, and virial RMSEs in the loss function were set to 1.0, 1.0, and 0.1, respectively.

C. Thermal conductivity calculations

We performed MD simulation using the GPUMD package (version 3.5)^{32,41} to calculate the LTCs for the two phases of Ga₂O₃. Based on the HNEMD method, the LTC can be calculated from the relation^{42,43}

$$\frac{\langle J^\mu(t) \rangle_{\text{ne}}}{TV} = \sum_v \kappa^{\mu\nu} F_e^v, \quad (1)$$

where $\kappa^{\mu\nu}$ is the thermal conductivity tensor, T is the system temperature, and V is the system volume. The non-equilibrium heat current $\langle J \rangle_{\text{ne}}$ is induced by the external driving force F_i^{ext} related to a driving-force parameter F_e with the dimension of inverse length⁴⁴

$$F_i^{\text{ext}} = F_e \cdot \mathbf{W}_i. \quad (2)$$

Here, \mathbf{W}_i is the virial tensor of atom i . The magnitude F_e of the driving-force parameter we used for both phases at different temperatures is small enough to keep the system within the linear-response regime. It should be noted that the HNEMD method is physically equivalent to the equilibrium molecular dynamics (EMD) method⁴⁵ (i.e., Green-Kubo method^{46,47}) but is much more computationally efficiently,^{43,48} which can predict length-independent thermal conductivity in the diffusive regime.

Moreover, the HNEMD method is adept at accounting for phonon anharmonicity to arbitrary order and incorporating phonon coherence effects.

All MD simulations were conducted at the target temperature using the Nose-Hoover chain method⁴⁹ with a time step of 1.0 fs. Initially, the simulation was run for 0.1 fs in the isothermal-isobaric ensemble and subsequently in the isothermal ensemble for 1.0 ns to achieve equilibrium. Afterward, HNEMD simulations were performed in the isothermal ensemble for 10.0 ns to calculate the running LTCs. We employed $4 \times 16 \times 8$ and $9 \times 5 \times 5$ supercells for β -Ga₂O₃ and κ -Ga₂O₃, respectively, containing 10 240 and 9000 atoms. The simulation sizes were validated to be sufficiently large to eliminate finite-size effects. For each case, the predicted LTC was calculated as the average of five independent simulations, and the corresponding standard error was also estimated.

III. RESULTS AND DISCUSSION

A. Validation of the NEP models

Figures 2(a)–2(c) show a comparison between the predicted energy, force, and virial values obtained from the NEP models and the corresponding DFT reference values for both the training and test sets of the two phases. In all scenarios, the RMSEs for energy, force, and virial are below 0.5 meV/atom, 40 meV/Å, and 5 meV/atom, respectively. These results demonstrate a very high accuracy of our NEP models. Additionally, in Fig. S2 of the [supplementary material](#), we present the energy changes in β -Ga₂O₃ and κ -Ga₂O₃ by employing single atom perturbation, as predicted by NEP and DFT. We randomly select an oxygen atom, move it along the [100] direction, and calculate the change in total energy. The predictions made by NEP models closely align with the results from DFT calculations, further demonstrating the precision of our developed NEP models. In addition to their high accuracy, our NEPs are remarkably efficient. For a system comprising 10 000 atoms, our NEPs can attain a computational speed of approximately 1.5×10^6 atom-step per second in the

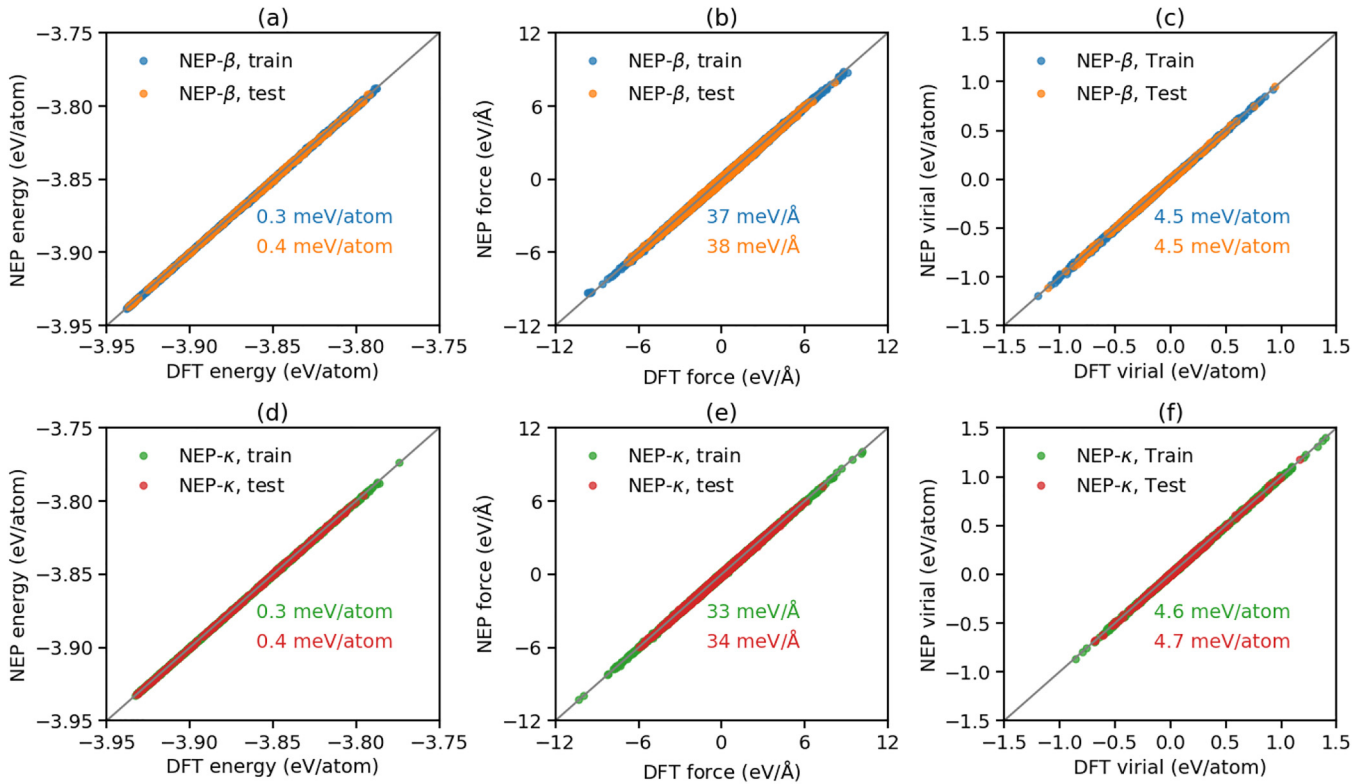


FIG. 2. The NEP predictions of [(a) and (d)] energy, [(b) and (e)] force, and [(c) and (f)] virial for the β -Ga₂O₃ (top) and κ -Ga₂O₃ (bottom) train and test sets against the DFT reference values.

GPUMD package using a single GeForce RTX 3090 GPU card. Compared with the BTE-ALD approach using SHENGBTE⁵⁰ package with force constants obtained from DFT calculations,⁵¹ our GPUMD + NEP approach is much more computationally efficient (see Fig. S2 of the [supplementary material](#)), which enables us to perform extensive simulations to study the LTCs of the Ga₂O₃ crystals.

B. Phonon dispersions

To assess the reliability of our NEP models in capturing the phonon transport properties of β -Ga₂O₃ and κ -Ga₂O₃, we compare the calculated phonon dispersions using both NEP and DFT methods, as shown in Fig. 3. It can be seen that for both phases, the acoustic branches predicted by NEP and DFT are very close, while the optical branches show slight deviations, especially at high frequencies. It should be noted that high-frequency optical phonons (>10 THz) contribute minimally to LTC,¹⁸ which is also confirmed by subsequent calculations of the spectrally decomposed LTC (see Fig. 6). Thus, we believe that the NEP models can reliably predict the LTC of the two phases of Ga₂O₃.

C. Thermal conductivity

After confirming the accuracy of the NEP models, we apply them to calculate LTCs using the HNEMD method. Figure 4 presents the LTC for both β - and κ -Ga₂O₃ using the HNEMD method at 300 K. Notably, Fig. 1(a) reveals that β -Ga₂O₃ possesses a monoclinic crystal structure, suggesting the potential for non-zero values in the off-diagonal elements in the LTC tensor. Fortunately, the HNEMD approach [see Eq. (1)] allows us to fully determine the LTC tensor as listed in Table I, by applying the external driving force along three orthogonal axes sequentially. As anticipated, the β phase exhibits minor couplings between the x and z directions. In contrast, the off-diagonal elements of the LTC tensor for the κ phase are zero, attributed to its orthorhombic crystal structure.

Based on the polar coordinates as shown in Fig. 5(a), we can determine the LTC along any crystal direction,⁵²

$$\kappa(\theta, \varphi) = \mathbf{a} \begin{pmatrix} \kappa_{xx} & \kappa_{xy} & \kappa_{xz} \\ \kappa_{xy} & \kappa_{yy} & \kappa_{yz} \\ \kappa_{xz} & \kappa_{yz} & \kappa_{zz} \end{pmatrix} \mathbf{a}^T, \quad (3)$$

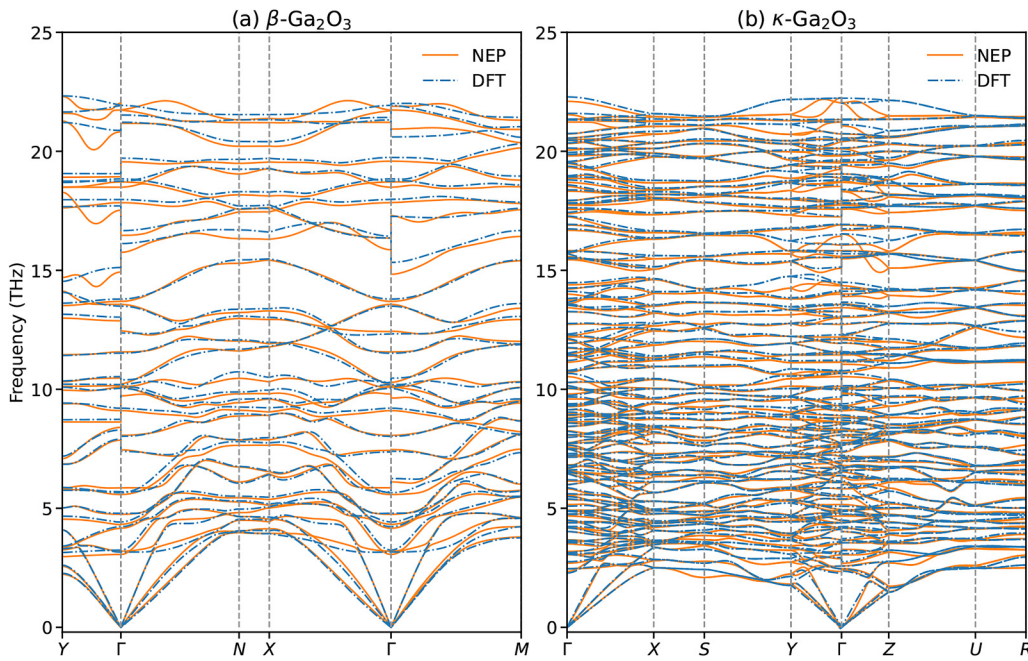


FIG. 3. The phonon dispersions of (a) β -Ga₂O₃ and (b) κ -Ga₂O₃ predicted by NEP and DFT. In order to accurately describe the splitting of LO-TO at the Γ point, NEP adopts the same method as DFT to add non-analytical terms of polar charge interaction to correct the dynamic matrix, that is, to provide the Born effective charges of each atom in the structure.

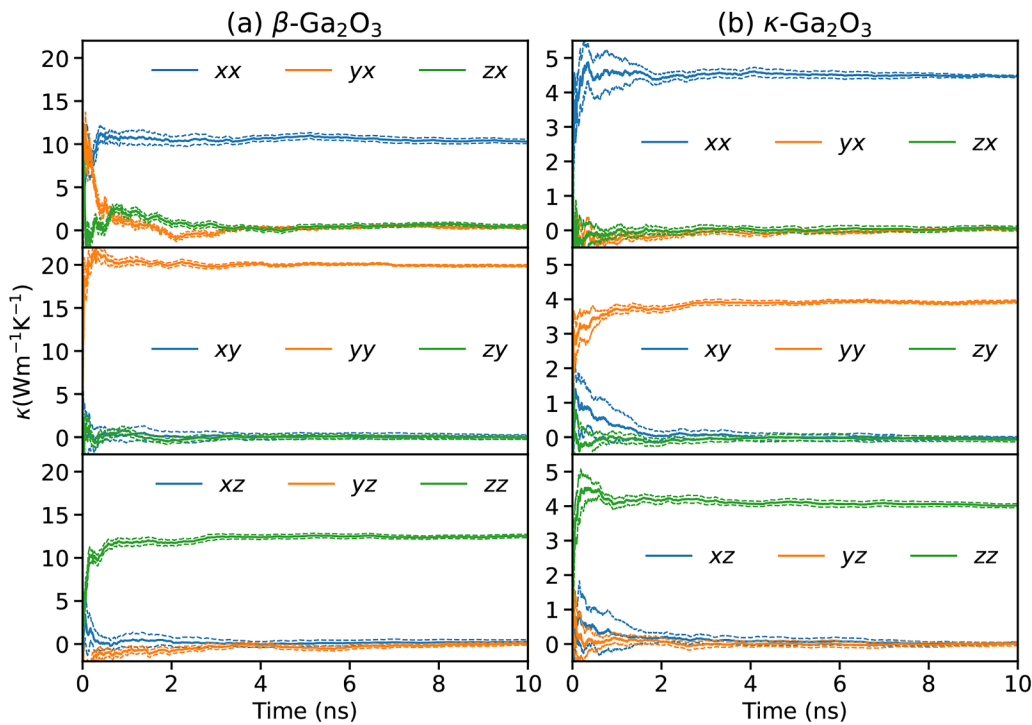


FIG. 4. Running LTC tensors from HNEMD simulations at 300 K for (a) β - and (b) κ -Ga₂O₃. Driving forces for top, middle, and bottom are along the x, y, and z directions, respectively.

23 February 2024 11:33:30

TABLE I. The predicted LTC tensor [W/(m K)] of (a) β -Ga₂O₃ and (b) κ -Ga₂O₃ from HNEMD simulations at 300 K.

LTC components	β -Ga ₂ O ₃	κ -Ga ₂ O ₃
κ_{xx}	10.3 (0.2)	4.5 (0.1)
κ_{yy}	19.9 (0.2)	3.9 (0.1)
κ_{zz}	12.5 (0.2)	4.0 (0.1)
κ_{xy}	0.2 (0.2)	0.0 (0.1)
κ_{xz}	0.4 (0.2)	0.0 (0.1)
κ_{yz}	0.0 (0.1)	0.0 (0.1)

with

$$\alpha = (\sin \varphi \cos \theta, \sin \varphi \sin \theta, \cos \varphi). \quad (4)$$

Figures 5(b) and 5(c) show the 3D distribution of LTC for the β and κ phases, respectively. The corresponding 2D projection in the [001], [010], and [100] planes is presented in Figs. 5(d)–5(f), respectively.

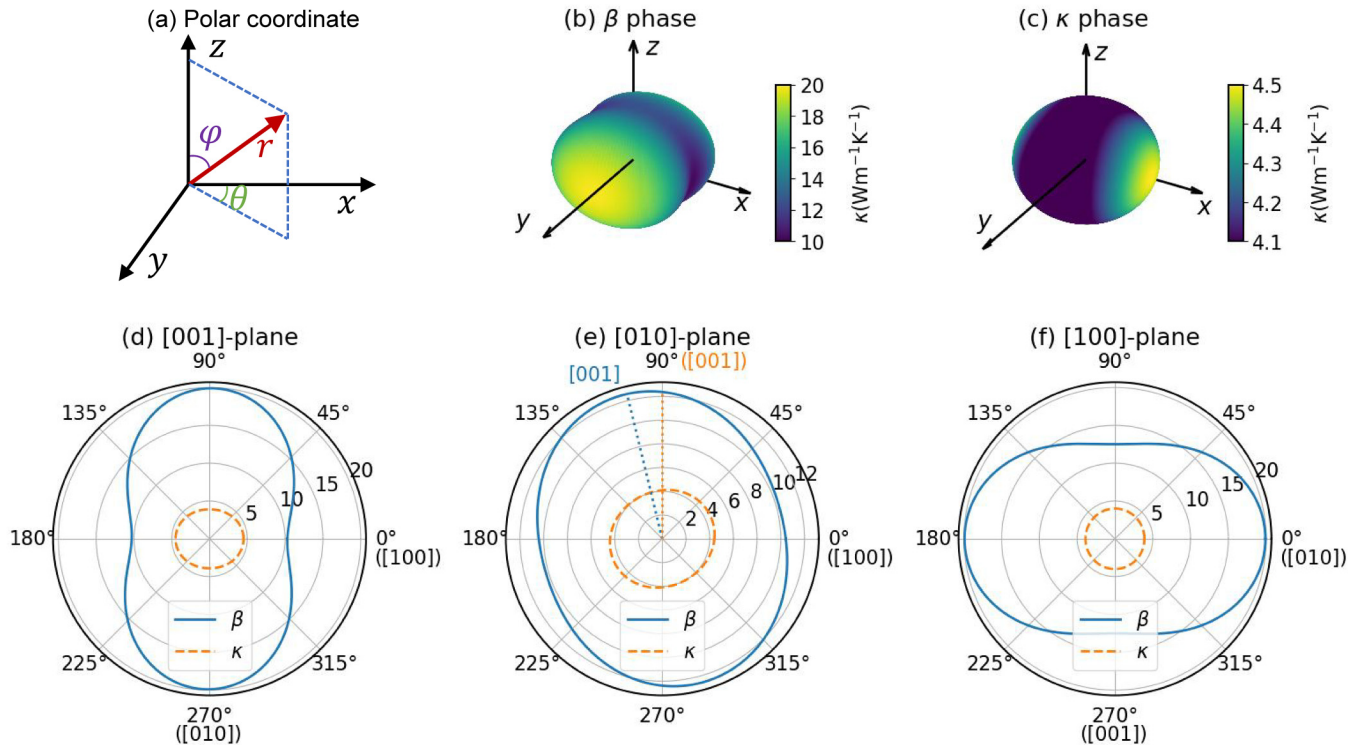
For the β phase, the LTC is highest along the [010] direction with 19.9 ± 0.2 W/(m K), followed by [001] with 12.6 ± 0.2 W/(m K) [see the blue dotted line in Fig. 5(e)] and [100] at 10.3 ± 0.2 W/(m K). As shown in Table II, our HNEMD results

TABLE II. The LTC [W/(m K)] of β -Ga₂O₃ at 300 K predicted by our HNEMD simulations and previously reported values. The values in parentheses denote the standard errors.

Method	[100]	[010]	[001]
Current HNEMD	10.3 (0.2)	19.9 (0.2)	12.6 (0.2)
Experiment ⁵²	9.5 (1.8)	22.5 (2.5)	13.3 (1.8)
Experiment ⁵³	10.9 (1.0)	27.0 (2.0)	15.0
EMD ¹⁵	10.7	20.8	12.6
EMD ²⁷	9.44	21.46	11.86
BTE-ALD ¹⁸	12.7	20.0	17.8
BTE-ALD ¹⁹	13.9	24.8	19.8
BTE-ALD ²⁰	10.02	23.74	12
BTE-ALD ⁵⁴	16.1	21.5	21.2
BTE-ALD ⁵¹	10.63	18.93	13.9

are consistent with previous experimental results^{52,53} using time-domain thermoreflectance and theoretical predictions based on the BTE-ALD method^{18–20,51,54} or the EMD method.^{15,27} This further demonstrates the reliability of our HNEMD approach based on machine-learned NEP in characterizing the LTC of Ga₂O₃ crystals.

Furthermore, we predict that the LTC for κ -Ga₂O₃ to be 4.5 ± 0.1 , 3.9 ± 0.1 , and 4.0 ± 0.1 W/(m K) along the [100],



23 February 2024 11:33:30

FIG. 5. (a) The polar coordination used for the transformation of the LTC tensor. (b) and (c) The 3D distributions of the LTC for β -Ga₂O₃ and κ -Ga₂O₃. [(d)–(f)] The corresponding 2D projections onto the [100], [010], and [001] planes, respectively. All LTCs are in units of W/(m K).

[010], and [001] directions, respectively. The results are consistent with those of a previous work which combines BTE with ALD to study the thermodynamic properties of Ga₂O₃.⁵¹ These values are about one-fifth to half of those of β-Ga₂O₃. While the β phase displays a significant LTC anisotropy with an anisotropy index of 1.94 [the maximum-to-minimum ratio of the LTC, see spatial distribution in Fig. 5(b)], the κ phase exhibits a nearly isotropic LTC pattern with an anisotropy index of 1.15 [see Fig. 5(c)].

To elucidate the disparities in the LTC observed between the two phases, we decomposed the LTC as a function of phonon frequency,⁴³

$$\kappa^{\mu\nu}(\omega) = \frac{2}{VTF_e^{\nu}} \int_{-\infty}^{\infty} dt e^{i\omega t} K^{\mu}(t). \quad (5)$$

Here, $K(t) = \sum_i (\mathbf{W}_i(0) \cdot \mathbf{v}_i(t))$ is the virial-velocity correlation function,⁴⁴ in which \mathbf{W}_i and \mathbf{v}_i are the virial tensor and the velocity of atom i , respectively.

Figure 6 presents the spectrally decomposed LTC of β-Ga₂O₃ and κ-Ga₂O₃ calculated from Eq. (5). Taken as a whole, only phonon modes with frequencies in the 0–10 THz range are really involved in thermal transport. It also can be found that, although in both phases the low-frequency acoustic phonons contribute significantly to the LTC, the β phase has a much broader distribution of phonon frequencies contributing to its LTC than the κ phase. This is also related to the phonon dispersions as shown in Fig. 3. The branches of the κ phase with a phonon frequency in the range of 5–10 THz are much flatter than those of the β phase, leading to much lower phonon group velocities. Moreover, in the κ phase, we observe significant overlaps between multiple bands for phonon

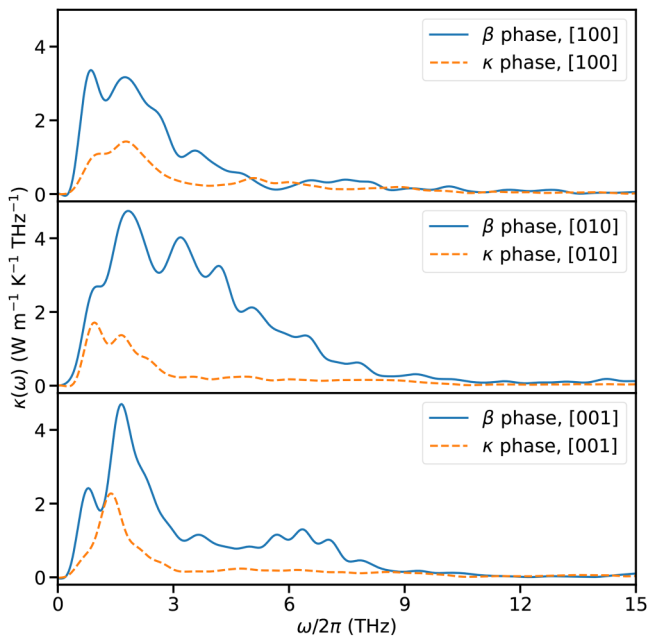


FIG. 6. The spectrally decomposed LTC of (a) β-Ga₂O₃ and (b) κ-Ga₂O₃ as a function of phonon frequency.

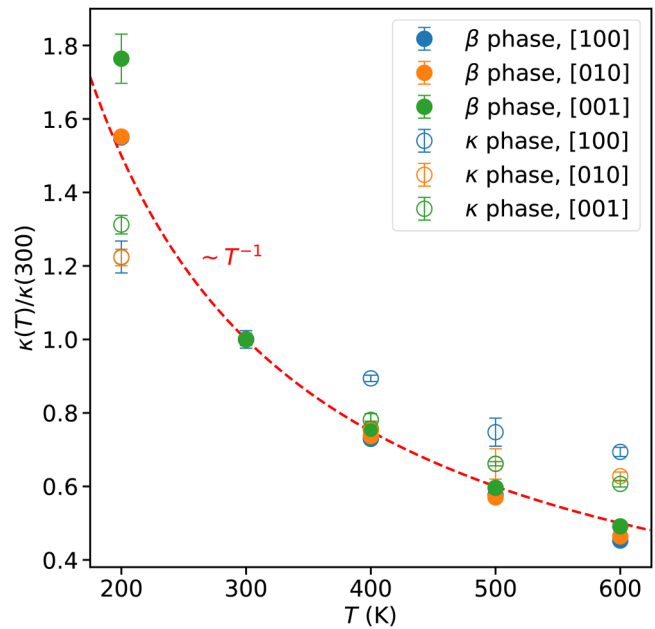


FIG. 7. LTC of β and κ phases of Ga₂O₃ as a function of temperature T along three directions. All the LTCs are normalized by their values at 300 K, respectively.

frequencies greater than 3 THz, indicating the presence of multiple scattering channels, a phenomenon previously observed in Violet phosphorene.²⁶

Furthermore, Fig. 7 shows the temperature-dependent LTC for β- and κ-Ga₂O₃. In the temperature range of 200–600 K, the LTCs of both phases decrease with increasing temperature. The LTC of the β phase exhibits a temperature dependence slightly stronger than $\sim T^{-1}$, as typical for systems dominated by three-phonon scattering processes.⁵⁵ However, the LTC of κ-Ga₂O₃ shows a clearly weaker temperature dependence, which is $\sim T^{-0.5}$ along the [100] direction and $\sim T^{-0.7}$ along the [010] and [001] directions, suggesting a significant impact of higher-order anharmonic phonon scatterings attributable to its complex crystal structures.⁵⁶

IV. CONCLUSIONS

In summary, we have developed machine-learned NEP models trained against quantum-mechanical DFT data for the β and κ phases of Ga₂O₃, which have been demonstrated to be accurate and efficient in predicting energy, atomic forces, virial, and phonon dispersions in both phases. Based on large-scale HNEMD simulations, we reached a consistent prediction with previous experimental measurements for the β phase and predicted the LTC of the κ phase. We found that the κ phase has a much lower LTC than the β phase, due to its phonon frequency contributions being limited to below 5 THz compared to the 0–10 THz range of the β phase. Furthermore, based on the tensor analysis, the κ phase exhibits an almost isotropic spatial distribution with an anisotropy index of

23 February 2024 11:33:30

1.15 at 300 K, in contrast to the pronounced anisotropy index of 1.94 for the β phase. We also examined the temperature dependence of the LTC in the two phases and found that the LTC of the β phase follows a temperature dependence slightly stronger than $\sim T^{-1}$, whereas the κ phase shows a weaker temperature dependence from $\sim T^{-0.5}$ to $\sim T^{-0.7}$, indicating a significant effect of high-order anharmonicity as in low-LTC materials. Our work demonstrates that the machine-learned NEP-driven HNEMD simulations can reliably and effectively characterize phonon thermal transport properties for complex crystals such as κ -Ga₂O₃, and thus we expect that this approach can be used to explore the LTCs of other phases of Ga₂O₃ as well.

SUPPLEMENTARY MATERIAL

See the supplementary material for the evolution of various loss functions during the training process, a comparison of computational efficiency between the GPUMD + NEP potential and the DFT + BTE-ALD method, and the validation of energy changes with single atom perturbation against DFT calculations.

ACKNOWLEDGMENTS

This work was supported by the Key-Area Research and Development Program of Guangdong Province (Grant No. 2020B010169002), the Guangdong Special Support Program (Grant No. 2021TQ06C953), and the Science and Technology Planning Project of Shenzhen Municipality (Grant No. JCYJ20190806142614541).

AUTHOR DECLARATIONS

Conflict of Interest

The authors have no conflicts to disclose.

Author Contributions

Xiaonan Wang: Data curation (lead); Formal analysis (lead); Investigation (equal); Methodology (equal); Software (equal); Visualization (lead); Writing – original draft (lead). **Jinfeng Yang:** Investigation (supporting); Methodology (supporting); Software (supporting); Writing – review & editing (supporting). **Penghua Ying:** Investigation (supporting); Methodology (equal); Software (equal); Validation (supporting); Writing – original draft (supporting); Writing – review & editing (supporting). **Zheyong Fan:** Methodology (supporting); Software (supporting); Writing – review & editing (equal). **Jin Zhang:** Writing – review & editing (supporting). **Huarui Sun:** Conceptualization (lead); Funding acquisition (lead); Project administration (lead); Resources (lead); Supervision (lead); Writing – review & editing (equal).

DATA AVAILABILITY

Complete input and output files for the NEP training of β -Ga₂O₃ and κ -Ga₂O₃ crystals are freely available at <https://gitlab.com/brucefan1983/nep-data>. The source code and documentation for GPUMD are available at <https://github.com/brucefan1983/GPUMD> and <https://gpumd.org>, respectively.

REFERENCES

- ¹S. Pearton, J. Yang, P. H. Cary, F. Ren, J. Kim, M. J. Tadjer, and M. A. Mastro, “A review of Ga₂O₃ materials, processing, and devices,” *Appl. Phys. Rev.* **5**, 011301 (2018).
- ²J. Zhang, P. Dong, K. Dang, Y. Zhang, Q. Yan, H. Xiang, J. Su, Z. Liu, M. Si, J. Gao *et al.*, “Ultra-wide bandgap semiconductor Ga₂O₃ power diodes,” *Nat. Commun.* **13**, 3900 (2022).
- ³N. Ueda, H. Hosono, R. Waseda, and H. Kawazoe, “Anisotropy of electrical and optical properties in β -Ga₂O₃ single crystals,” *Appl. Phys. Lett.* **71**, 933–935 (1997).
- ⁴M. Orita, H. Ohta, M. Hirano, and H. Hosono, “Deep-ultraviolet transparent conductive β -Ga₂O₃ thin films,” *Appl. Phys. Lett.* **77**, 4166–4168 (2000).
- ⁵P. Feng, J. Y. Zhang, Q. H. Li, and T. H. Wang, “Individual β -Ga₂O₃ nanowires as solar-blind photodetectors,” *Appl. Phys. Lett.* **88**, 153107 (2006).
- ⁶X. Zhou, M. Li, J. Zhang, L. Shang, K. Jiang, Y. Li, L. Zhu, J. Chu, and Z. Hu, “Flexible solar-blind photodetectors based on β -Ga₂O₃ films transferred by a stamp-based printing technique,” *IEEE Electron Device Lett.* **43**, 1921–1924 (2022).
- ⁷W. S. Hwang, A. Verma, H. Peelaers, V. Protasenko, S. Rouvimov, A. Seabaugh, W. Haensch, C. V. de Walle, Z. Galazka, M. Albrecht *et al.*, High-voltage field effect transistors with wide-bandgap β -Ga₂O₃ nanomembranes,” *Appl. Phys. Lett.* **104**, 203111 (2014).
- ⁸S. J. Pearton, F. Ren, M. Tadjer, and J. Kim, “Perspective: Ga₂O₃ for ultra-high power rectifiers and MOSFETs,” *J. Appl. Phys.* **124**, 220901 (2018).
- ⁹H. Y. Playford, A. C. Hannon, E. R. Barney, and R. I. Walton, “Structures of uncharacterised polymorphs of gallium oxide from total neutron diffraction,” *Chem. Eur. J.* **19**, 2803–2813 (2013).
- ¹⁰Y. Zhuo, Z. Chen, W. Tu, X. Ma, Y. Pei, and G. Wang, “ β -Ga₂O₃ versus ϵ -Ga₂O₃: Control of the crystal phase composition of gallium oxide thin film prepared by metal-organic chemical vapor deposition,” *Appl. Surf. Sci.* **420**, 802–807 (2017).
- ¹¹I. Cora, F. Mezzadri, F. Boschi, M. Bosi, M. Čaplovičová, G. Calestani, I. Dófony, B. Pécz, and R. Fornari, “The real structure of ϵ -Ga₂O₃ and its relation to κ -phase,” *CrystEngComm* **19**, 1509–1516 (2017).
- ¹²B. M. Janzen, P. Mazzolini, R. Gillen, V. F. Peltason, L. P. Grote, J. Maultzsch, R. Fornari, O. Bierwagen, and M. R. Wagner, “Comprehensive raman study of orthorhombic κ/ϵ -Ga₂O₃ and the impact of rotational domains,” *J. Mater. Chem. C* **9**, 14175–14189 (2021).
- ¹³Y. Chen, H. Ning, Y. Kuang, X.-X. Yu, H.-H. Gong, X. Chen, F.-F. Ren, S. Gu, R. Zhang, Y. Zheng *et al.*, “Band alignment and polarization engineering in κ -Ga₂O₃/GaN ferroelectric heterojunction,” *Sci. China Phys. Mech. Astron.* **65**, 277311 (2022).
- ¹⁴S. Krishna, Y. Lu, C.-H. Liao, V. Khandelwal, and X. Li, “Band alignment of orthorhombic Ga₂O₃ with GaN and AlN semiconductors,” *Appl. Surf. Sci.* **599**, 153901 (2022).
- ¹⁵R. Li, Z. Liu, A. Rohskopf, K. Gordiz, A. Henry, E. Lee, and T. Luo, “A deep neural network interatomic potential for studying thermal conductivity of β -Ga₂O₃,” *Appl. Phys. Lett.* **117**, 152102 (2020).
- ¹⁶X. Wan, D. Ma, D. Pan, L. Yang, and N. Yang, “Optimizing thermal transport in graphene nanoribbon based on phonon resonance hybridization,” *Mater. Today Phys.* **20**, 100445 (2021).
- ¹⁷L. Yang, X. Wan, D. Ma, Y. Jiang, and N. Yang, “Maximization and minimization of interfacial thermal conductance by modulating the mass distribution of the interlayer,” *Phys. Rev. B* **103**, 155305 (2021).
- ¹⁸Z. Yan and S. Kumar, “Phonon mode contributions to thermal conductivity of pristine and defective β -Ga₂O₃,” *Phys. Chem. Chem. Phys.* **20**, 29236–29242 (2018).
- ¹⁹Y. Liu, J. Yang, G. Xin, L. Liu, G. Csányi, and B. Cao, “Machine learning interatomic potential developed for molecular simulations on thermal properties of β -Ga₂O₃,” *J. Chem. Phys.* **153**, 144501 (2020).
- ²⁰Y. Chen, L. Peng, Y. Wu, C. Ma, A. Wu, H. Zhang, and Z. Fang, “Anomalous temperature-dependent phonon anharmonicity and strain engineering of thermal conductivity in β -Ga₂O₃,” *J. Phys. Chem. C* **127**, 13356–13363 (2023).

- ²¹X. Wan, W. Feng, Y. Wang, H. Wang, X. Zhang, C. Deng, and N. Yang, "Materials discovery and properties prediction in thermal transport via materials informatics: A mini review," *Nano Lett.* **19**, 3387–3395 (2019).
- ²²Y. Wang, Z. Fan, P. Qian, M. A. Caro, and T. Ala-Nissila, "Quantum-corrected thickness-dependent thermal conductivity in amorphous silicon predicted by machine learning molecular dynamics simulations," *Phys. Rev. B* **107**, 054303 (2023).
- ²³H. Zhang, X. Gu, Z. Fan, and H. Bao, "Vibrational anharmonicity results in decreased thermal conductivity of amorphous HfO₂ at high temperature," *Phys. Rev. B* **108**, 045422 (2023).
- ²⁴T. Liang, P. Ying, K. Xu, Z. Ye, C. Ling, Z. Fan, and J. Xu, "Mechanisms of temperature-dependent thermal transport in amorphous silica from machine-learning molecular dynamics," *Phys. Rev. B* **108**, 184203 (2023).
- ²⁵P. Ying, T. Liang, K. Xu, J. Zhang, J. Xu, Z. Zhong, and Z. Fan, "Sub-micrometer phonon mean free paths in metal-organic frameworks revealed by machine learning molecular dynamics simulations," *ACS Appl. Mater. Interfaces* **15**, 36412–36422 (2023).
- ²⁶P. Ying, T. Liang, K. Xu, J. Xu, Z. Fan, T. Ala-Nissila, and Z. Zhong, "Variable thermal transport in black, blue, and violet phosphorene from extensive atomistic simulations with a neuroevolution potential," *Int. J. Heat Mass Transfer* **202**, 123681 (2023).
- ²⁷Z. Sun, Z. Qi, K. Liang, X. Sun, Z. Zhang, L. Li, Q. Wang, G. Zhang, G. Wu, and W. Shen, "A neuroevolution potential for predicting the thermal conductivity of α , β , and ϵ -Ga₂O₃," *Appl. Phys. Lett.* **123**, 192202 (2023).
- ²⁸J. Zhao, J. Byggmästar, H. He, K. Nordlund, F. Djurabekova, and M. Hua, "Complex Ga₂O₃ polymorphs explored by accurate and general-purpose machine-learning interatomic potentials," *npj Comput. Mater.* **9**, 159 (2023).
- ²⁹Y. Liu, H. Liang, L. Yang, G. Yang, H. Yang, S. Song, Z. Mei, G. Csányi, and B. Cao, "Unraveling thermal transport correlated with atomistic structures in amorphous gallium oxide via machine learning combined with experiments," *Adv. Mater.* **35**, 2210873 (2023).
- ³⁰Z. Fan, Z. Zeng, C. Zhang, Y. Wang, K. Song, H. Dong, Y. Chen, and T. Ala-Nissila, "Neuroevolution machine learning potentials: Combining high accuracy and low cost in atomistic simulations and application to heat transport," *Phys. Rev. B* **104**, 104309 (2021).
- ³¹Z. Fan, "Improving the accuracy of the neuroevolution machine learning potential for multi-component systems," *J. Phys.: Condens. Matter* **34**, 125902 (2022).
- ³²Z. Fan, Y. Wang, P. Ying, K. Song, J. Wang, Y. Wang, Z. Zeng, K. Xu, E. Lindgren, J. M. Rahm, A. J. Gabourie, J. Liu, H. Dong, J. Wu, Y. Chen, Z. Zhong, J. Sun, P. Erhart, Y. Su, and T. Ala-Nissila, "GPUMD: A package for constructing accurate machine-learned potentials and performing highly efficient atomistic simulations," *J. Chem. Phys.* **157**, 114801 (2022).
- ³³P. E. Blöchl, "Projector augmented-wave method," *Phys. Rev. B* **50**, 17953 (1994).
- ³⁴J. P. Perdew, K. Burke, and M. Ernzerhof, "Generalized gradient approximation made simple," *Phys. Rev. Lett.* **77**, 3865 (1996).
- ³⁵G. Kresse and J. Furthmüller, "Efficient iterative schemes for ab initio total-energy calculations using a plane-wave basis set," *Phys. Rev. B* **54**, 11169 (1996).
- ³⁶G. Kresse and D. Joubert, "From ultrasoft pseudopotentials to the projector augmented-wave method," *Phys. Rev. B* **59**, 1758 (1999).
- ³⁷A. Togo and I. Tanaka, "First principles phonon calculations in materials science," *Scr. Mater.* **108**, 1–5 (2015).
- ³⁸J. Åhman, G. Svensson, and J. Albertsson, "A reinvestigation of β -gallium oxide," *Acta Crystallogr., Sect. C: Cryst. Struct. Commun.* **52**, 1336–1338 (1996).
- ³⁹R. Drautz, "Atomic cluster expansion for accurate and transferable interatomic potentials," *Phys. Rev. B* **99**, 014104 (2019).
- ⁴⁰T. Schaul, T. Glasmachers, and J. Schmidhuber, "High dimensions and heavy tails for natural evolution strategies," in *Proceedings of the 13th Annual Conference on Genetic and Evolutionary Computation, GECCO '11* (Association for Computing Machinery, New York, 2011), pp. 845–852.
- ⁴¹Z. Fan, W. Chen, V. Vierimaa, and A. Harju, "Efficient molecular dynamics simulations with many-body potentials on graphics processing units," *Comput. Phys. Commun.* **218**, 10–16 (2017).
- ⁴²D. J. Evans, "Homogeneous NEMD algorithm for thermal conductivity—application of non-canonical linear response theory," *Phys. Lett. A* **91**, 457–460 (1982).
- ⁴³Z. Fan, H. Dong, A. Harju, and T. Ala-Nissila, "Homogeneous nonequilibrium molecular dynamics method for heat transport and spectral decomposition with many-body potentials," *Phys. Rev. B* **99**, 064308 (2019).
- ⁴⁴A. J. Gabourie, Z. Fan, T. Ala-Nissila, and E. Pop, "Spectral decomposition of thermal conductivity: Comparing velocity decomposition methods in homogeneous molecular dynamics simulations," *Phys. Rev. B* **103**, 205421 (2021).
- ⁴⁵X. Gu, Z. Fan, and H. Bao, "Thermal conductivity prediction by atomistic simulation methods: Recent advances and detailed comparison," *J. Appl. Phys.* **130**, 210902 (2021).
- ⁴⁶M. S. Green, "Markoff random processes and the statistical mechanics of time-dependent phenomena. II. Irreversible processes in fluids," *J. Chem. Phys.* **22**, 398–413 (1954).
- ⁴⁷R. Kubo, "Statistical-mechanical theory of irreversible processes. I. General theory and simple applications to magnetic and conduction problems," *J. Phys. Soc. Jpn.* **12**, 570–586 (1957).
- ⁴⁸P. Ying, T. Liang, Y. Du, J. Zhang, X. Zeng, and Z. Zhong, "Thermal transport in planar sp²-hybridized carbon allotropes: A comparative study of biphenylene network, pentaheptite and graphene," *Int. J. Heat Mass Transfer* **183**, 122060 (2022).
- ⁴⁹M. E. Tuckerman, *Statistical Mechanics: Theory and Molecular Simulation* (Oxford University Press, 2023).
- ⁵⁰W. Li, J. Carrete, N. A. Katcho, and N. Mingo, "Shengbte: A solver of the Boltzmann transport equation for phonons," *Comput. Phys. Commun.* **185**, 1747–1758 (2014).
- ⁵¹J. Yang, Y. Xu, X. Wang, X. Zhang, Y. He, and H. Sun, "Lattice thermal conductivity of β -, α - and κ -Ga₂O₃: A first-principles computational study," *Appl. Phys. Express* **17**, 011001 (2023).
- ⁵²P. Jiang, X. Qian, X. Li, and R. Yang, "Three-dimensional anisotropic thermal conductivity tensor of single crystalline β -Ga₂O₃," *Appl. Phys. Lett.* **113**, 232105 (2018).
- ⁵³Z. Guo, A. Verma, X. Wu, F. Sun, A. Hickman, T. Masui, A. Kuramata, M. Higashiwaki, D. Jena, and T. Luo, "Anisotropic thermal conductivity in single crystal β -Ga₂O₃," *Appl. Phys. Lett.* **106**, 111909 (2015).
- ⁵⁴M. D. Santia, N. Tandon, and J. Albrecht, "Lattice thermal conductivity in β -Ga₂O₃ from first principles," *Appl. Phys. Lett.* **107**, 041907 (2015).
- ⁵⁵L. Lindsay, D. A. Broido, and T. L. Reinecke, "Ab initio thermal transport in compound semiconductors," *Phys. Rev. B* **87**, 165201 (2013).
- ⁵⁶L. Lindsay, A. Katre, A. Cepellotti, and N. Mingo, "Perspective on ab initio phonon thermal transport," *J. Appl. Phys.* **126**, 050902 (2019).